

Contents lists available at [SciVerse ScienceDirect](#)

Journal of Nuclear Materials

journal homepage: www.elsevier.com/locate/jnucmat

Effect of $n = 3$ perturbation field amplitudes below the ELM triggering threshold on edge and SOL transport in NSTX

J.D. Lore^{a,*}, J.M. Canik^a, J.-W. Ahn^a, A. Bortolon^b, E.D. Fredrickson^c, M.A. Jaworski^c, G.J. Kramer^c, R. Maingi^{a,1}, A.G. McLean^d, F. Scotti^c, V.A. Soukhanovskii^d, K. Tritz^e

^aOak Ridge National Laboratory, Oak Ridge, TN 37831, USA

^bUniversity of California-Irvine, Irvine, CA 92697, USA

^cPrinceton Plasma Physics Laboratory, Princeton, NJ 08543, USA

^dLawrence Livermore National Laboratory, Livermore, CA 94550, USA

^eJohns Hopkins University, Baltimore, MD 21287, USA

ARTICLE INFO

Article history:

Available online xxxxx

ABSTRACT

The pulsed application of $n = 3$ magnetic perturbation fields with amplitudes below that which triggers ELMs results in distinct, transient responses observable on several edge and divertor diagnostics in NSTX. We refer to these responses as Sub-Threshold Edge Perturbations (STEPs). An analysis of edge measurements suggests that STEP s result in increased transport in the plasma edge and scrape-off layer, which leads to augmentation of the intrinsic strike point splitting due to error fields, i.e., an intensification of the helical divertor footprint flux pattern. These effects are much smaller in magnitude than those of triggered ELMs, and are observed for the duration of the field perturbation measured internal to the vacuum vessel. In addition, STEP s are correlated with changes to the MHD activity, along with transient reductions in the neutron production rate. Ideally the STEP s could be used to provide density control and prevent impurity accumulation, in the same manner that on-demand ELM triggering is used on NSTX, without the impulsive divertor fluxes and potential for damage to plasma facing components associated with ELMs.

Published by Elsevier B.V.

1. Introduction

The application of small non-axisymmetric magnetic field perturbations has been found to significantly affect edge plasma transport and stability in tokamaks. Applied non-axisymmetric fields are now regularly used to control edge localized modes (ELMs) on a large number of devices [1–6]. On NSTX, previous experiments have demonstrated paced triggering of ELMs [7,8] and modification of the divertor heat and particle fluxes [9,10] with $n = 3$ applied field perturbations. It was shown that paced ELM triggering allows for control over the secular density rise and impurity accumulation in otherwise ELM-free H-modes. On the other hand, a significant fraction of the plasma stored energy is lost during each ELM, even at the maximum possible triggered ELM frequency. The maximum triggering frequency is limited in the current system by vessel eddy currents as the perturbation coils are external to the vacuum vessel. The divertor heat and particle load during an ELM may become a problem in future

devices, such as the planned NSTX-Upgrade [11]. To mitigate or eliminate these deleterious effects, it is important to pursue techniques which may lead to density control and reduced impurity accumulation in plasmas free of large ELMs.

One possible route to such an operating scenario is through the pulsed application of $n = 3$ perturbation fields of an amplitude and duration below that which causes ELMs to be triggered. It has been shown in previous experiments that ELMs are triggered by perturbation fields at NSTX when the applied pulse exceeds a certain ‘threshold’ that is a function of the pulse length and magnitude, as well as the plasma configuration [12]. That is, if the pulse amplitude (or duration) is continually decreased compared to a waveform that causes reliable ELM triggering, ELMs are destabilized only infrequently, and finally no ELMs are triggered. In this paper we do not attempt to quantify the parameters of this threshold, however we will refer to perturbation field waveforms as sub-threshold, meaning that ELMs are triggered infrequently or not at all. It was found that perturbation field pulses near the threshold generate a small transport response even when an ELM is not triggered. We refer to these transport responses as Sub-Threshold Edge Perturbations (STEPs). A characterization of the STEP s, measurable on several edge and scrape-off-layer (SOL) diagnostics is presented here.

* Corresponding author. Address: Oak Ridge National Laboratory, 1 Bethel Valley Rd., Oak Ridge, TN 37831, USA.

E-mail addresses: lorejd@ornl.gov (J.D. Lore), rmaingi@pppl.gov (R. Maingi).

¹ Presenting author.

2. Experimental setup

In NSTX, 3D field pulses are applied using a midplane coil set normally used for error field correction and resistive wall mode (RWM) feedback control [13]. In the experiments discussed here, these ‘RWM coils’ have been configured to apply an $n = 3$ field. The coils are external, but close fitting, to the vacuum vessel. Eddy currents induced in the vessel cause the internal field perturbation to lag the coil current waveform. Fig. 1a shows the coil current waveform for two different pulse trains: 6 ms square pulses (black, solid line) and 3 ms square pulses (blue², dot-dashed line). The internal field perturbation is measured by magnetic sensors located ~ 10 cm from the plasma, and peaks at the end of the current pulse (Fig. 1b). The perturbed field amplitude decays over ~ 10 ms. The addition of a current spike of the opposite sign at the end of the pulse can greatly reduce the decay time (see Fig. 2a).

Several pulse trains that did not result in the regular triggering of ELMs have been investigated. Above a nominal current amplitude, ~ 1 kA, STEPs are measurable. One case is examined in detail below, with the effect of other pulse duration and amplitudes discussed briefly at the end of Section 3.1. NSTX Discharge 138146 was configured to have 3 ms, 2 kA square pulses applied at 40 Hz (Fig. 1, dashed blue line). The pulses are used in addition to the $n = 3$ error field correction, but as will be shown in Section 3, ‘intrinsic’ strike point splitting is observed due to error fields. These discharges have lithium wall coatings, with 200 mg of lithium injected per shot, and are free of ELMs in the absence of 3D fields. The plasmas are near double null, with $\delta_r^{sep} \sim -5$ mm, where δ_r^{sep} is the radial distance between the separatrices at the outboard midplane, with high triangularity $\delta = 0.8$, and moderate elongation $\kappa \sim 2.3$. The toroidal field strength $B_t = -0.5$ T, with $I_p \sim 800$ kA, and 4 MW of neutral beam power injected.

3. Characterization of STEP responses

The application of non-axisymmetric fields is known to affect both the transport and stability of tokamak plasmas. Generally, even small levels of asymmetry can lead to increased collisional transport, rotation damping, and the creation of magnetic islands and stochastic field regions [14]. In NSTX, the application of $n = 3$ pulses above a threshold level results in robust and controllable triggering of ELMs and modification to the kinetic profiles in the pedestal region [7,8]. The pulses have also been observed to trigger an enhanced confinement regime known as enhanced pedestal H-mode [15] in NSTX. In addition, 3D fields alter divertor heat and particle flux profiles through augmentation of the intrinsic strike point splitting and changes in the recycling properties in NSTX [8,9] and other tokamaks [16–19].

On NSTX, applying $n = 3$ pulses near the ELM triggering threshold level results in unreliable triggering, as shown in Fig. 2. The pulses that do not trigger ELMs nevertheless cause STEPs, measurable in, e.g., the D_α light (Fig. 2b), radiated power (Fig. 2c) and soft X-ray emission from the plasma edge (Fig. 2d) and the neutron production rate (Fig. 2e). The effects of a STEP can be broadly divided into two categories, changes to the edge, SOL, and divertor transport; and modification of the MHD activity, followed by a drop in the neutron production rate. The time response of the former is generally proportional to the internal field perturbation, approximately symmetric in time, peaking at internal field maximum. The modification of the magnetohydrodynamic (MHD) activity occurs on a faster timescale, ~ 0.1 – 0.3 ms after the application of the $n = 3$ fields, accompanied by the reduction in

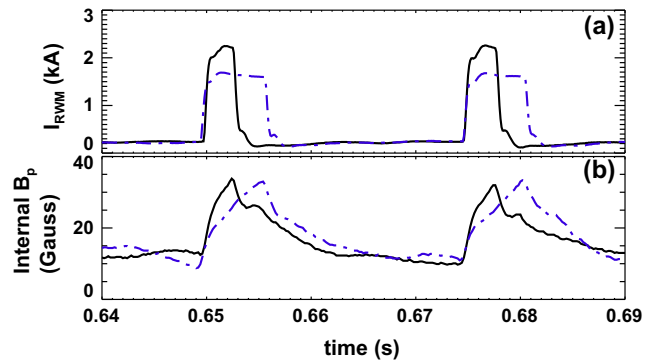


Fig. 1. (a) RWM coil current waveforms and (b) internal magnetic measurements showing the lag of internal field perturbation due to vessel eddy currents.

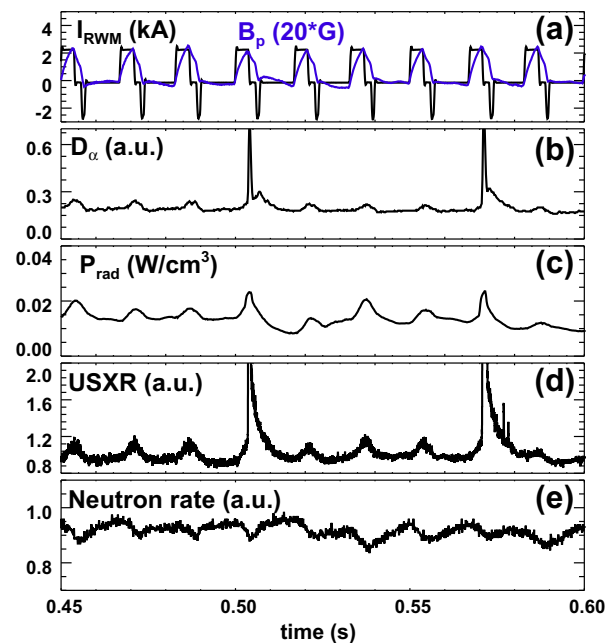


Fig. 2. (a) RWM coil current and internal magnetic field perturbation resulting in both triggered ELMs and STEPs. Effects are visible on (b) D_α emission, (c) radiated power, (d) USXR light, and (e) neutron production.

the neutron rate. STEPs are clearly distinct from triggered ELMs, both in magnitude and timescale.

3.1. Effect of STEPs on edge, SOL, and divertor transport

Fig. 3 shows the D_α emission measured by (a) 1D CCD camera and (b) a filterscope viewing the divertor. During this time window no ELMs are triggered. Each $n = 3$ pulse results in a $\sim 50\%$ increase in D_α emission and ‘augmentation’ of the intrinsic strike point splitting, i.e., a general increase in the magnitude and number of observable flux peaks. The maximum in the D_α signal occurs at the maximum of the internal field perturbation. Two radial profiles are shown in Fig. 4, during the pulse (blue) and between pulses (black). The pulses generally result in a small reduction in the primary peak ($R \sim 32$ cm), while the other profile peaks due to the error fields are increased in magnitude. Additional peaks are observed near $R = 52$ and 61 cm. We interpret these measurements as evidence of a topological field structure that occurs from the superposition of the vacuum applied $n = 3$ fields and the

² For interpretation of color in Figs. 1 and 6, the reader is referred to the web version of this article.

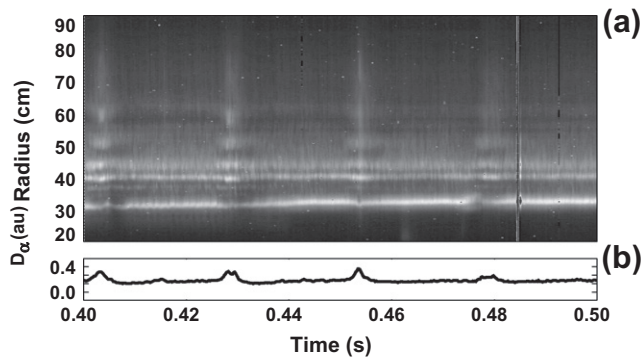


Fig. 3. D_α measurements from (a) 1D CCD divertor camera, (b) divertor filterscope showing augmented strike point splitting due to STEPs.

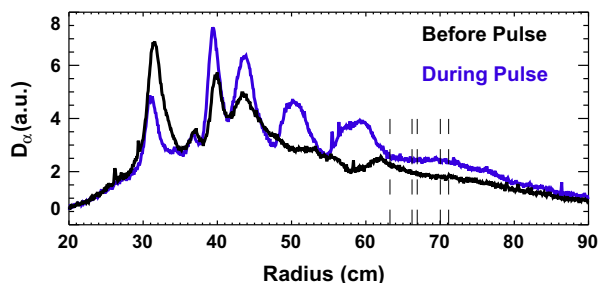


Fig. 4. Radial profiles of D_α emission between 3D field pulses (black, $t = 424$ ms) and during a pulse (blue, $t = 428$ ms). Dashed lines indicate divertor probe radii. (For interpretation of the references to color in this figure legend, the reader is referred to the web version of this article.)

axisymmetric equilibrium fields. In this ‘vacuum approximation’ the axisymmetric separatrix is split into stable and unstable manifolds [14], resulting in a 3D field structure where fieldlines followed from within the unperturbed separatrix trace out a series of helical lobes that intersect the divertor plates in a striated pattern [9,16–19]. Higher fluxes are expected where long connection length fieldlines guide heat and particles from the pedestal region to the divertor. This structure and the resulting divertor patterns exist *before* the application of the perturbation fields due to error fields in these discharges, i.e., the invariant manifolds are decomposed before the STEP. The STEPs result in an augmentation of the divertor fluxes, suggesting increased transport into the SOL resulting in the lobes being ‘filled’ with hotter plasma increasing the measured emission. As the error fields are also dominantly $n = 3$, a gross change in the lobe structure due to the applied fields is not expected [10]. The striated pattern is clearly shown in Fig. 5, viewed by a Phantom camera filtered for D_α light [20]. Fig. 5 shows the augmentation of the intrinsic splitting directly, the ‘background’ emission before the $n = 3$ pulse application has been subtracted from the emission during the pulse.

Fig. 6 shows the ion saturation current measured by a radial array of triple probes located at the lower divertor ($R = 63\text{--}71$ cm).

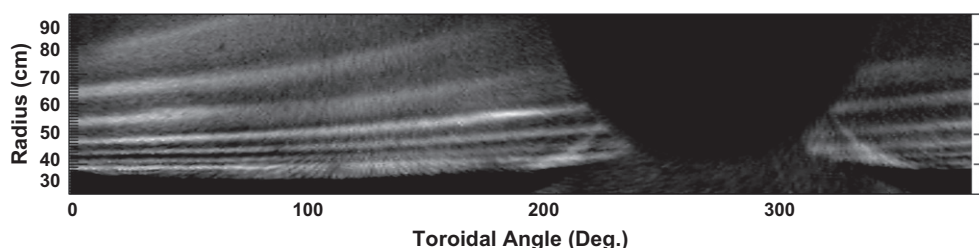


Fig. 5. Strike point splitting due to a STEP; emission before the pulse has been subtracted.

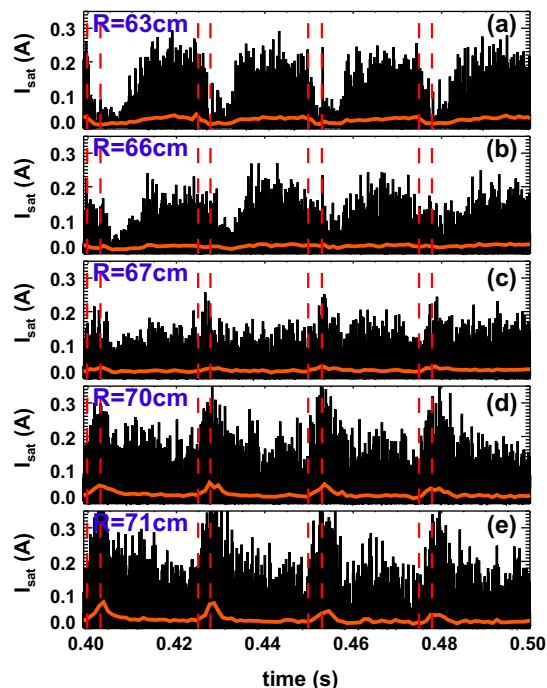


Fig. 6. Divertor particle flux measured by a triple probe array at the lower divertor. Each STEP results in a modification that varies with radial position.

For these high triangularity plasmas the probes are located in the far-SOL region. The $n = 3$ pulse times are indicated by vertical dashed red lines. At the inner radii, the ‘grassy’ behavior and the average current (1 ms average, orange line), decrease during and immediately following the pulses. At the outer radii the magnitude of the spikes and the average current increases. The radial location of the probes is indicated by vertical dashed lines in Fig. 4. The fluctuations in the far-SOL indicate a highly skewed distribution of fluxes, a common characteristic in turbulent plasmas [21], and the different behavior as a function of radius suggests that the $n = 3$ pulses are affecting the turbulence properties.

Regular perturbations are also observed on several chords of an ultrasoft X-ray (USXR) imaging system viewing in a poloidal array and a bolometer array viewing toroidally along the midplane. The outermost USXR signal is shown in Fig. 7c, and an edge bolometer chord in Fig. 7b. The effects are localized to the outer chords of both systems ($\psi_N > 0.5$, where $\psi_N = (\psi(R, Z) - \psi_{axis}) / (\psi_{sep} - \psi_{axis})$ is evaluated at the point of tangency). While the radiated power in several edge chords shows regular modulations correlated with the $n = 3$ pulses, no significant impact in the total volume integrated radiated power is observed.

The STEP behavior described above is also observed for RWM coil square pulses of different duration and amplitude. The duration of the STEP response is linearly proportional to the duration of the applied field. In general, a larger RWM coil current

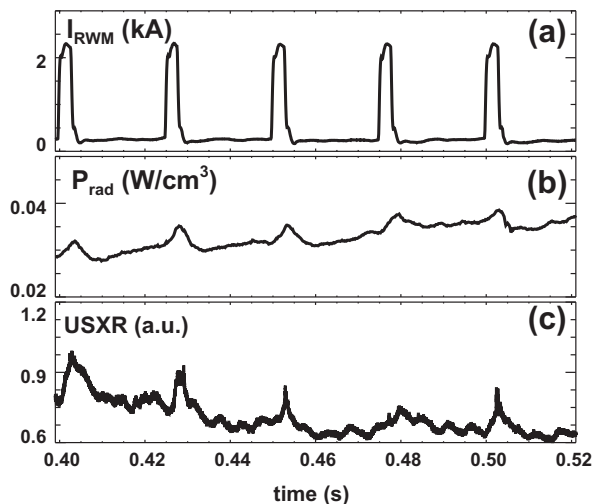


Fig. 7. (a) RWM coil current, (b) radiated power, and (c) USX light for discharge 138,146.

amplitude results in a larger STEP response, e.g., a larger increase in the USXR intensity. The effect of different waveforms will be examined in a future experiment.

3.2. Effects on neutron production and MHD activity

In these experiments the neutron production rate, measured by a fission chamber, shows a regular modulation (Fig. 8b). At each STEP, the neutron rate transiently drops by $\sim 5\%$ over a ~ 5 ms period (comparable with the $n = 3$ pulse duration), and then recovers on a longer timescale (10–20 ms). As TRANSP [22] calculations show that the neutron production in NSTX is mostly due to beam–target reactions ($\sim 85\%$), the observed drops suggest that STEPs may influence confinement of beam ions. This is also indicated by the response of the activity of MHD modes in the 0.5–1.5 MHz range of frequencies, thought to be Compressional and/or Global Alfvén Eigenmodes [23]. These are plasma modes, destabilized through resonance with beam ions. Changes in the bursting frequency and mode amplitude are observed (Fig. 8c), possibly associated to a modification of the fast ion drive. STEPs can affect

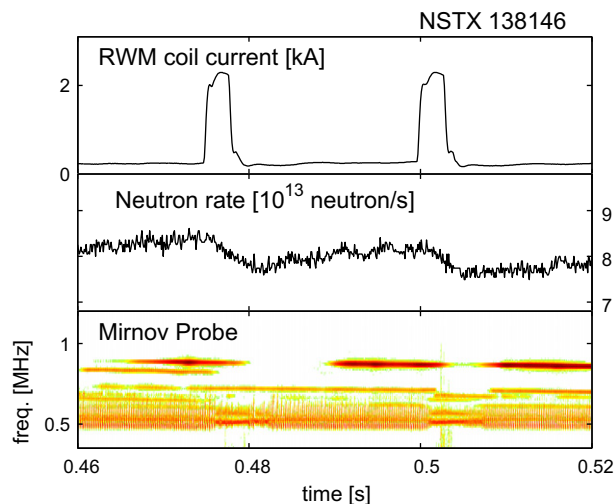


Fig. 8. (a) RWM coil current, (b) neutron rate, and (c) spectrogram of a Mirnov probe signal in the 0.5–1.0 MHz frequency range, showing the bursting/chirping MHD activity from CAE/GAE modes.

fast ion confinement through (1) modification of the background kinetic profiles and consequently beam ion birth profile; (2) perturbation of the fast-ion orbits. The experimental observations and preliminary analysis is presented here for completeness; quantifying these effects is an area of ongoing research and will be presented in a future paper.

4. Comparison to triggered ELMs

The responses discussed in Section 3 are distinct from those from triggered ELMs. As shown in Fig. 2, the STEP precedes the ELM by several milliseconds. The STEPs are generally symmetric in time, while the D_α and USXR responses to a triggered ELM have a fast onset and slow decay. The magnitude of the change in the D_α , P_{rad} , and USXR signals is larger during a triggered ELM. In addition, the effects are observed in each USXR and bolometer chord, not localized to the outer channels. Triggered ELMs generally result in measurable changes in global quantities, such as electron and carbon density, kinetic stored energy, and total radiated power. In addition, the triggered ELM response appears to be superimposed over the responses described in Section 3a, e.g., the increases in the D_α and USXR signals occur before the ELM is triggered. The effects described in Section 3.2 are independent of the triggered ELMs.

5. Discussion and summary

The application of non-axisymmetric field amplitudes below the ELM triggering threshold results in regular, distinct responses measurable by several edge, SOL, and divertor diagnostics. Each STEP produces effects that suggest an increase in edge transport, e.g., increases in D_α and USXR emission and increased ion saturation current measured by divertor probes. The split flux patterns to the divertor plates are intensified during a STEP, as measured by divertor cameras and probe arrays. This effect is interpreted as an augmentation of the strike point splitting due to error fields, i.e., the existing lobe structure in the magnetic field is filled in by the increased transport into the SOL. Ideally the 3D field pulses would be used to provide density control and prevent impurity accumulation while avoiding the triggering of ELMs. The tested pulse trains, however, did not result in significant changes to the global plasma quantities. While most of the effects appear to be localized to the plasma edge, the $n = 3$ pulses may also affect the core plasma as indicated by the concurrent modulation of high frequency MHD modes and reduction in the neutron production rate. These latter effects are currently under investigation by means of full-orbit simulations.

Acknowledgment

This work is supported by U.S. Department of Energy Contract Numbers DE-AC05-00OR22725 and DE-AC02-09CH11466.

References

- [1] T. Shoji et al., J. Nucl. Mater. 196 (1992) 296.
- [2] T.E. Evans et al., Phys. Rev. Lett. 92 (2004) 235003.
- [3] S.M. Kaye et al., Phys. Rev. Lett. 98 (2007) 175002.
- [4] Y. Liang et al., Phys. Rev. Lett. 98 (2007) 265004.
- [5] W. Suttrop et al., Phys. Rev. Lett. 106 (2011) 225004.
- [6] J. Kim et al., Nucl. Fusion 52 (2012) 114011.
- [7] J.M. Canik et al., Phys. Rev. Lett. 104 (2010) 045001.
- [8] J.M. Canik et al., Nucl. Fusion 50 (2010) 064016.
- [9] J.-W. Ahn et al., Nucl. Fusion 50 (2010) 045010.
- [10] J.-W. Ahn et al., Phys. Plasmas 18 (2011) 056108.
- [11] A. Loarte et al., Plasma Phys. Control. Fusion (2007).
- [12] J.M. Canik et al., Nucl. Fusion 50 (2010) 034012.
- [13] S.A. Sabbagh et al., Phys. Rev. Lett. 97 (2006) 045004.

- [14] T.E. Evans et al., *Chaos, Complexity and Transport: Theory and Applications*, World Scientific, Singapore, 2008.
- [15] R. Maingi et al., *Phys. Rev. Lett.* 105 (2010) 135004.
- [16] T. Evans et al., *J. Phys.: Conf. Ser.* 7 (2005) 174.
- [17] M.W. Jakubowski et al., *Nucl. Fusion* 49 (2009) 095013.
- [18] E. Nardon et al., *J. Nucl. Mater.* 415 (2011) S914.
- [19] D.M. Harting et al., *Nucl. Fusion* 52 (2012) 054009.
- [20] F. Scotti et al., *Rev. Sci. Instr.* 83 (2012) 10E532.
- [21] S. Zweben et al., *Plasma Phys. Control. Fusion* 49 (2007) S1.
- [22] R.J. Hawryluk, *Physics of plasmas close to thermonuclear conditions*, in: B. Coppi et al. (Eds.), *Proceedings of the International School of Plasma Physics*, vol. 1, Pergoma, New York, 1980, p. 19.
- [23] E.D. Fredrickson et al., *Phys. Plasmas* 13 (2006) 056109.